This manuscript was accepted by J. Chem. Phys. Click here to see the version of record.

Metal doping in cerium metal-organic frameworks for visible-response water splitting photocatalysts

Xin-Ping Wu (吴新平),[a)] Laura Gagliardi,[a)] and Donald G. Truhlar[a)]

Department of Chemistry, Chemical Theory Center, and Minnesota Supercomputing Institute, University of Minnesota, Minneapolis, Minnesota 55455-0431, USA.

[a)]Authors to whom correspondence should be addressed. Electronic addresses: xwuphd@umn.edu, gagliard@umn.edu, and truhlar@umn.edu.

ABSTRACT: Cerium metal-organic frameworks (MOFs) show great promise for photocatalytic water splitting as they have low-lying unoccupied 4*f* orbitals with energies lower than the unoccupied linker orbitals to drive the ligand-to-metal charge transfer (LMCT) of the photo-generated electron at the linker to separate the photo-excited charges. Nevertheless, the large and negative LMCT energies of Ce-MOFs are often accompanied by high photon-absorption energies, which then limits the application of Ce-MOFs as visible-light-driven water splitting photocatalysts. In this work, we propose that metal (Zr or Ti) doping can raise the very negative LMCT energies of Ce-MOFs, consequently leading to the decrease of the absorption energy and promoting the response of Ce-MOFs to visible light. By functionalizing the linker of the mixed-metal MOFs, we found two possible visible-response photocatalysts for water splitting using a single photocatalyst.

I. INTRODUCTION

Hydrogen (H_2) has several characteristics making it a favorable species for energy storage and supply.[1] One attractive characteristic of hydrogen is that it only produces water upon oxidation; therefore, hydrogen is a clean energy source. Among various production pathways, photocatalytic conversion of solar energy to hydrogen through photocatalytic water splitting shows great promise.[2,3,4,5] Therefore, in the past few decades, great efforts have been devoted to investigating water-splitting photocatalysts, with special emphasis on oxides such as TiO_2,[6,7,8] and in recent years, an increasing number of studies have focused on photocatalytic metal-organic frameworks (MOFs), a class of nanoporous organic–inorganic crystalline materials.[8,9,10]

MOFs are modularly composed of two kinds of building blocks, namely inorganometallic nodes and the organic linkers.[11] The broad tunability of MOFs is promoted by the large variety of possibilities for the node, the linker, and the net topology that arranges them into a periodic structure,[11] and one hopes to be able to use this for fine-tuning of the electronic structure to drive specific photocatalytic reactions.[12] In addition, the porous nature and high surface area of MOFs facilitate the diffusion and adsorption of reactants.[10,13,14] Accordingly, MOFs are promising candidates for photocatalyst design.

For photocatalytic water splitting, stability in a humid vapor or in the aqueous phase is required, but only a subset of MOFs have such stability;[15] among them is UiO-66 with $Zr_6O_4(OH)_4$ nodes and 1,4-benzene-dicarboxylate (BDC) linkers.[16,17] It has been reported that the Zr ions in the nodes of UiO-66 can be completely substituted by Hf, Th, U, or Ce;[18,19,20,21,22] partial metal substitution (i.e., metal doping) in the nodes with metals such as Ti or Ce to form a mixed-metal node can be achieved as well;[23,24,25,26,27,28,29,30] the pure-metal and mixed-metal derivatives often can maintain the water stability of the original Zr-UiO-66.[18,20,23,28,29] Therefore, the use of UiO-66 derivatives as water splitting photocatalysts has raised great interest.[9,31,32,33]

Photoexcitation of UiO-66 MOFs generally occurs on the linker. Recently, we studied the electronic structures of the UiO-66 MOFs with Zr, Hf, Th, Ti, U, or Ce as the metal ion in the node, and we found that, of the systems studied, only Ce-substituted UiO-66 has exoergic ligand-to-metal charge transfer (LMCT) after photon excitation of the linker, that is, it has a negative ligand-to-metal charge-transfer energy E_{LMCT}, which is defined as the energy change upon transferring an electron from the photoexcited linker orbital to the lowest unoccupied metal ion orbital.[34] The negative E_{LMCT} of Ce-UiO-66 is due to the empty 4*f* orbitals of the Ce ions lying lower than the photoexcited linker orbital (the lowest unoccupied linker orbital).[34]

A key to efficient photocatalysis is facile separation of electrons from holes and long lifetime of the separated pair. The negative E_{LMCT} Ce-UiO-66 means that long-lived charge-separated excited-states can be expected, with the hole on the linker and the electron on the metal ion.[34] These results are consistent with a recent study.[35] We also found that the favorable LMCT of the Ce-UiO-66 can be preserved after linker functionalization.[34] Therefore, we predicted that functionalized Ce-UiO-66 frameworks are potential photocatalysts.[34]

However, these Ce-UiO-66 frameworks always have a high photon-absorption energy E_{abs}, which is defined as the energy change upon exciting an electron from the highest occupied linker orbital to the lowest unoccupied linker orbital. For Ce-UiO-66 frameworks, the highest occupied linker orbital is the highest occupied crystal orbital (HOCO) and the lowest unoccupied 4*f* orbital is the lowest unoccupied crystal orbital (LUCO), so the high E_{abs} is correlated with a very negative E_{LMCT} (~ -1.4 eV) since

$$E_{abs} = E_g - E_{LMCT} \quad (1)$$

where E_g is the HOCO–LUCO gap. The high E_{abs} means that visible photons will not be absorbed.[34] Our proposal was to lower E_{abs} by raising E_{LMCT} (making it less negative) by functionalizing the BDC linkers with electron-withdrawing groups.[34]

In the present article, we propose an alternative strategy to lower E_{abs} based on doping the $Ce_6O_4(OH)_4$ node of Ce-UiO-66 with Zr or Ti. The reasons for choosing Zr and Ti as the doping ions are that (i) CeO_2 is able to form solid solutions with ZrO_2 and TiO_2,[36,37] (ii) mixed Ce/Zr-UiO-66 has been successfully synthesized,[25,29] and (iii) Ti doping in Zr-UiO-66 is feasible;[23,24,26,27,28,30] therefore Ti doping in Ce-UiO-66 is probably feasible as well. By performing Kohn-Sham density functional theory (DFT) calculations, we show that Zr or Ti doping in Ce-UiO-66 can tune the photocatalytic properties (i.e., E_{abs}, E_{LMCT}, and E_g) of the framework. In particular, metal doping can engineer the band gap, lower the photon-absorption

energy, and raise the LMCT energy. We consider various options for linker functionalization on the mixed-metal MOFs to search for visible-light photo-active materials.

II. COMPUTATIONAL METHODS

The primitive cell is shown in yellow in Figure 1, and it was employed to perform spin-polarized periodic DFT calculations by using the *Vienna ab initio Simulation Package* (*VASP*).[38,39] The PBEsol[40] and HSE06[41] exchange–correlation functionals were applied for geometry optimizations and single-point calculations (to obtain energies and electronic properties), respectively. We refer to this protocol as HSE06//PBEsol, and we have previously validated it for predicting both the equilibrium lattice constants and the electronic properties of UiO-66-type materials.[34]

The core electrons were treated by using the projector augmented wave (PAW) method[42] with a kinetic energy cutoff of 500 eV and with H (1*s*), C (2*s*, 2*p*), N (2*s*, 2*p*), O (2*s*, 2*p*), S (3*s*, 3*p*), Br (4*s*, 4*p*), I (5*s*, 5*p*), Ti (3*s*, 3*p*, 4*s*, 3*d*), Zr (4*s*, 4*p*, 5*s*, 4*d*), and Ce (5*s*, 5*p*, 6*s*, 5*d*, 4*f*) electrons being treated as valence states. A 3×3×3 *k*-point mesh sampling was used for geometry optimizations, and a 1×1×1 *k*-point mesh sampling (i.e., Γ point sampling of the first Brillouin zone) was used for single-point calculations; the latter has been shown to be sufficient in previous studies.[43,44] The convergence criterion for SCF iterations was 10^{-5} eV. Both atomic positions and the shape of the cell were allowed to relax during optimization, for which we used a Hellman–Feynman force criterion of 0.02 eV/Å on each ion.

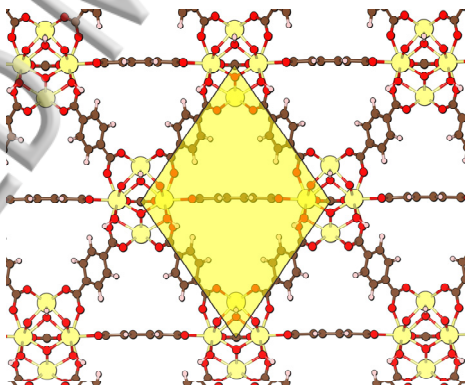

FIG. 1. The framework structure of Ce-UiO-66. The primitive cell is indicated by a yellow background. Color scheme: Ce, yellow; O, red; C, brown; H, light pink (this color scheme is used throughout the paper).

The isolated O_2 and H_2 molecules were simulated using 20×20×20 $Å^3$ cells. For calculations on O_2 molecule, H_2 molecule, graphite, cerium metal, zirconium metal, and titanium metal, we used a kinetic energy cutoff of 500 eV and *k*-point mesh samplings of 5×5×5, 5×5×5, 8×8×3, 4×4×4,

6×6×4, and 7×7×5, respectively. The HSE06//PBEsol protocol was used for calculations on these structures to obtain the energies.

To align the electronic energies to the vacuum level, the method developed by Butler et al.[45] was used; specifically, the vacuum reference potential was estimated by the average potential of a spherical probe (radius: 1 Å) at the center of the large octahedral cage (~11 Å) of a UiO-66 framework. Our previous work confirmed that the method is reliable for MOF UiO-66.[34]

Calculations on isolated H_2BDC-type species were performed using *Gaussian 16*.[46] The ground-state structures were optimized by relaxing all the atoms by HSE06. Then excited-state calculations were performed on the ground-state structures (vertical transitions) using time-dependent density functional theory (TD-DFT) with the adiabatic linear-response approximation.[47] For both ground-state and excited-state calculations, we used the HSE06 exchange–correlation functional with the def2-TZVP[48,49] basis set. The vertical transitions of isolated H_2BDC-type species were transformed to simulated absorption spectra by *GaussView 6.0.16*[50] using a Gaussian line shape with a standard deviation of 0.4 eV.

III. RESULTS AND DISCUSSION

A. Doping Configurations

For mixed Ce/M-UiO-66 MOFs, we use the notation Ce-UiO-66(M_n), where M is the doping atom (i.e., Zr or Ti) and n is the number of doping ions per node ($1 \leq n \leq 5$). (The special case of $n = 0$ is Ce-UiO-66, and the special case of $n = 6$ is M-UiO-66.) In all of these species, each metal has the formal oxidation state +4.

Figure 2 shows the node structure of Ce-UiO-66, in which the six Ce sites are equivalent. To search the stable structures for n from 1 to 5, we considered nine possible doping configurations, i.e., (1), (1,2), (1,3), (1,2,3), (1,3,5), (1,3,6), (1,2,3,4), (1,2,3,5), and (1,2,3,4,5) where the numbers separated by commas and enclosed by parentheses are the doping sites identified by the labels in Figure 2. Therefore, isostructures exist when $n = 2$, 3, and 4, that is, only one possible doping configuration exists when n is 1 or 5, while for $n = 2$ or 4, two distinct doping configurations exist, and for $n = 3$, three distinct doping configurations exist.

Table I gives the relative energies of the isostructural Ce-UiO-66(Zr_n) and Ce-UiO-66(Ti_n) when $n = 2$, 3, or 4. The table shows that Ce-UiO-66(Zr_n) and Ce-UiO-66(Ti_n) have the same most stable doping configurations for $n = 2$, 3, or 4, namely (1,3) for $n = 2$, (1,3,6) for $n = 3$, and (1,2,3,5) for $n = 4$; for $n = 3$, the energy of configuration (1,3,5) is very close to that of configuration (1,3,6) for both Zr and Ti doping, probably because they have similar structures with the only difference being the species centered at the triangle constituted by the three doping atoms, i.e., OH species for configuration (1,3,5) and O ion for configuration (1,3,6). These results also suggest that the doping atoms tend to be packed closely together.

This manuscript was accepted by J. Chem. Phys. Click here to see the version of record.

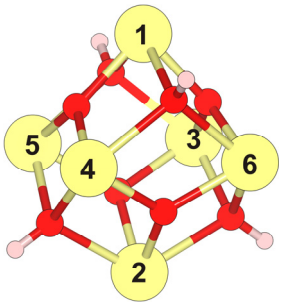

FIG. 2. The $Ce_6O_4(OH)_4$ node of Ce-UiO-66. The six Ce sites are labeled with numbers.

TABLE I. Relative energies (ΔE, in eV) of isostructural Ce-UiO-66(M_n) with M = Zr or Ti when n = 2, 3, or 4

n		2		3			4	
doping configuration		(1,2)	(1,3)	(1,2,3)	(1,3,5)	(1,3,6)	(1,2,3,4)	(1,2,3,5)
ΔE	M = Zr	0.36	0	0.38	0.01	0	0.40	0
	M = Ti	0.79	0	0.97	0.05	0	1.26	0

The primitive cell has only one node per cell, while the unit cell has four nodes. Therefore, doping in a unit cell (or an even larger supercell) creates many more possible doping configurations than doping in a primitive cell. However, the additional possibilities can be estimated as different combinations of the nine considered doping configurations. Accordingly, the primitive cell is expected to be adequate to simulate mixed-metal UiO-66.

B. Solid Stability and Potential Synthesis

We know of no mixed Ce/Ti-UiO-66 MOFs having been reported in the literature. Therefore, they should be considered at present as hypothetical MOFs, and it is necessary to investigate their stabilities. The energy of formation for a material is widely used as a quantity to assess solid stability,[51,52,53] and we use this quantity here to discuss the stabilities of mixed-metal MOFs.

The energy of formation of Ce-UiO-66(M_n) is the energy of this reaction:

$$(6\text{-}n)\text{Ce(s)} + n\text{M(s)} + 16\text{O}_2\text{(g)} + 48\text{C(s, graphite)} + 14\text{H}_2\text{(g)} \rightarrow \text{Ce-UiO-66(M}_n\text{)(s)}$$

Accordingly, the energy of formation (E_f) is given in eV/(metal atom) by

$$E_f = \{E_{\text{Ce-UiO-66(M}_n\text{)}} - [(6-n)E_{\text{Ce}} + nE_{\text{M}} + 16E_{\text{O}_2} + 48E_{\text{C}} + 14E_{\text{H}_2}]\}/6$$

where $E_{\text{Ce-UiO-66(M}_n\text{)}}$, E_{Ce}, E_{M}, E_{O_2}, E_{C}, E_{H_2} are the DFT calculated electronic energies for a Ce-UiO-66(M_n) primitive cell, a Ce atom in cerium metal, a Zr or Ti atom in bulk metal, a gas-phase O_2 molecule, a C atom in graphite, and a gas-phase H_2 molecule, respectively, and the denominator is the number of metal atoms in a Ce-UiO-66(M_n) primitive cell.

Table II shows that the calculated energies of formation for the most stable configurations of Ce-UiO-66(Zr_n) and Ce-UiO-66(Ti_n) have large negative values, indicating the stability of the UiO-66 framework with respect to the elements in their standard states. Formation from the elements in their standard states is of course not sufficient to ensure stability, but we will use these energies of formation to calculate the energy of producing the mixed-metal MOFs from two pure-metal MOFs.

Figure 3 shows the energies of formation of the pure-metal and mixed-metal MOFs. The black dashed line in the figure connects the energies of formation of Ce-UiO-66 and Zr-UiO-66 and the blue one connects the energies of formation of Ce-UiO-66 and Ti-UiO-66; therefore, the deviation of the energy of formation from its corresponding dashed line is the energy change of mixing two different pure-metal MOFs to form a mixed-metal MOF. We see that for both the Zr and the Ti cases the energies of formation for the mixed-metal MOFs are slightly above the dashed line, therefore the energies of mixing are small and positive; they are tabulated in Table II. In the language of phase stability studies,[54,55] the mixed-metal species are not on the convex hull. This is consistent with a previous computational study[56] on mixed Ce/Zr-UiO-66 MOFs.

The energies of mixing being positive would correspond to the mixed phases being less stable than separated pure phases. However, although a full calculation of the phase stability would involve free energies, we and the previous study[56] both simply used the electronic energies (because the phonon calculations necessary to compute free energies are computationally very demanding). The free energy change upon mixing is expected to be less positive or negative because the entropic term that we did not calculate favors a solid solution over single-component phases.[57] Furthermore, it is known that thermodynamically metastable structures can be synthetically accessible because they can be kinetically stable. One relevant example is that mixed Ce/Zr-UiO-66 MOFs have already been synthesized in experiments.[25,29] Therefore, we expect that mixed Ce/Ti-UiO-66 MOFs can also be synthesized since their energies of mixing are comparable to those of mixed Ce/Zr-UiO-66 MOFs (see Table II). It may also be relevant that, as we stated above, CeO_2 can form solid solutions with ZrO_2 and TiO_2,[36,37] and this further supports the argument that the mixed Ce/Ti-UiO-66 MOFs may be synthetically feasible.

TABLE II. Summary of energies of formation (E_f, in eV/(metal atom)) and energies of mixing (E_{mix}, in eV/(metal atom)) for the most stable configurations of Ce-UiO-66(M_n) (M = Zr or Ti; n is the number of M per node)

		$n = 0$	$n = 1$	$n = 2$	$n = 3$	$n = 4$	$n = 5$	$n = 6$
M = Zr	E_f	-21.011	-20.946	-20.913	-20.907	-20.863	-20.849	-20.871
	E_{mix}	0	0.042	0.052	0.034	0.055	0.046	0
M = Ti	E_f	-21.011	-20.532	-20.120	-19.796	-19.404	-19.076	-18.861
	E_{mix}	0	0.121	0.174	0.140	0.173	0.143	0

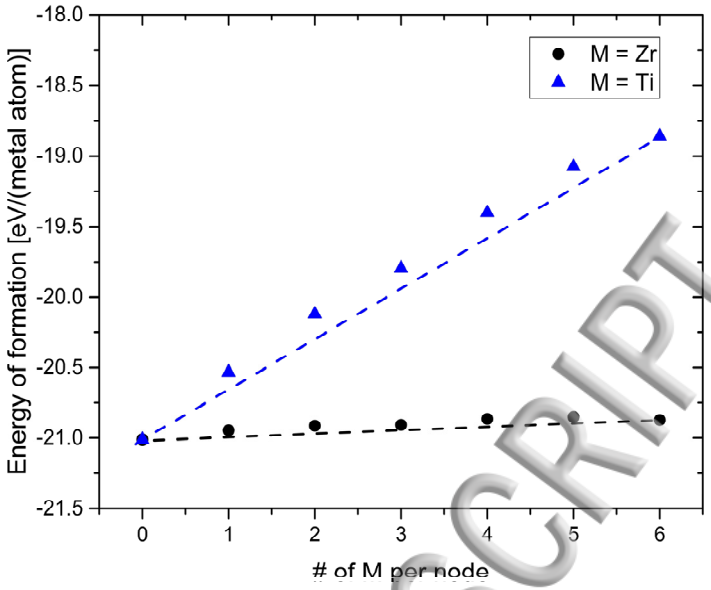

FIG. 3. Energies of formation for the most stable configurations of Ce-UiO-66(M_n) (M = Zr or Ti; *n* is the number of M per node). The dashed lines represent the linear change of the energy of formation from the pure Ce-UiO-66 to the pure M-UiO-66.

C. Electronic Structures of Mixed-Metal MOFs

The photocatalytic process in Ce-based UiO-66 (e.g., pure Ce-UiO-66 with or without linker functionalization) involves (i) linker excitation upon light absorption, (ii) electron transfer from the photo-excited linker to the node via LMCT, which leads to the separation of photo-excited charges (electrons and holes), and (iii) photocatalytic reaction driven by excited electrons and holes.[34] Step (i) is favorable in unsubstituted or substituted Ce-UiO-66 because excitation occurs on the linker. The efficiency of step (i) is correlated with the absorption energy (E_{abs}); E_{abs} in the range 1.7-3.2 eV is necessary to utilize the visible range of solar radiation. Step (ii) is favorable in unsubstituted or substituted Ce-UiO-66 because they have negative E_{LMCT} due to the low-lying empty 4*f* orbitals. Therefore, having Ce^{4+} ions in a MOF leads to a negative E_{LMCT}. Because of eq 1, the very negative E_{LMCT} (−1.43 eV)[34] in pure Ce-UiO-66 needs to be raised moderately, preferably to be a negative value that above −1 eV, in order to utilize the visible light. For step (iii), as already discussed in our previous work,[34] the HOCO–LUCO gap and the absolute HOCO and LUCO positions need to be considered. For example, for photocatalytic water splitting using a single photocatalyst, an appropriate HOCO–LUCO gap (E_g) is required to straddle the energy levels of the catalyzed redox couple. For the oxygen evolution reaction (OER), $H_2O \leftrightarrow 2H^+(aq) + \frac{1}{2}O_2(g) + 2e^-$, and the hydrogen evolution reaction (HER), $2H^+(aq) + 2e^- \leftrightarrow H_2(g)$, the energy level of HOCO should be lower than the OER level while the energy level of LUCO should be higher than the HER level.

The most stable and the second most stable doping configurations of Ce-UiO-66(M_3) (M = Zr or Ti) have very close relative energies (see Table I). We compared their electronic structures, and

they are very similar (see Figures S1 and S2 in the Supplementary Material). Thus we will continue to base our discussion on the most stable configuration.

Figure 4 shows the density of states (DOS) of the most stable configurations of Ce-UiO-66(Zr$_n$) and Ce-UiO-66(Ti$_n$) and also the E_{abs} and E_{LMCT} for each case (note that for Zr-UiO-66 and Ti-UiO-66, E_{LMCT} is 2.00 and 0 eV, respectively, because Zr 4*d* orbitals are high in energy and Ti 3*d* orbitals mix effectively with the unoccupied linker orbitals). It should be noted that for the mixed-metal cases, even though there is a second metal, E_{LMCT} is still the energy change from the lowest unoccupied linker orbital to the lowest unoccupied 4*f* orbital – just as for Ce-UiO-66 – because, according to the definition, E_{LMCT} is associated with the lowest unoccupied metal orbital, and in the mixed-metal cases the lowest unoccupied metal orbital is a Ce 4*f* orbital.

For Zr or Ti doping in Ce-UiO-66, we found that, with increased doping (increasing *n*), the position of the lowest unoccupied linker orbital gradually shifts towards HOCO, which is probably because Zr 4*d* and Ti 3*d* orbitals are better than Ce 4*f* orbitals for mixing with the unoccupied linker orbitals (see Figure S3 in the Supplementary Material). The width of the Ce 4*f* band decreases as the Ce ions mix less with linker orbitals (see Figure 4). These considerations lead to the increase of E_{LMCT} and the decrease of E_{abs} with increasing *n* (see Figure 4). Since Ti 3*d* orbitals can hybridize more effectively than Zr 4*d* orbitals with the unoccupied linker orbitals (see Figure S3 in the Supplementary Material), doping with Ti has stronger effects on E_{abs} and E_{LMCT} than doping with Zr. But doping either Zr or Ti into a Ce-MOF has promise for making a visible-response water-splitting photocatalyst. Figure 4 also shows that the HOCO–LUCO gap changes as a result of doping. For Zr doping, the HOCO–LUCO gap is continuously opened when increasing the doping concentration. In the case of Ti doping, the HOCO–LUCO gap is slightly lowered at low doping concentration, while it is opened when the Ti:Ce ratio is equal to or higher than 1.

This manuscript was accepted by J. Chem. Phys. Click here to see the version of record.

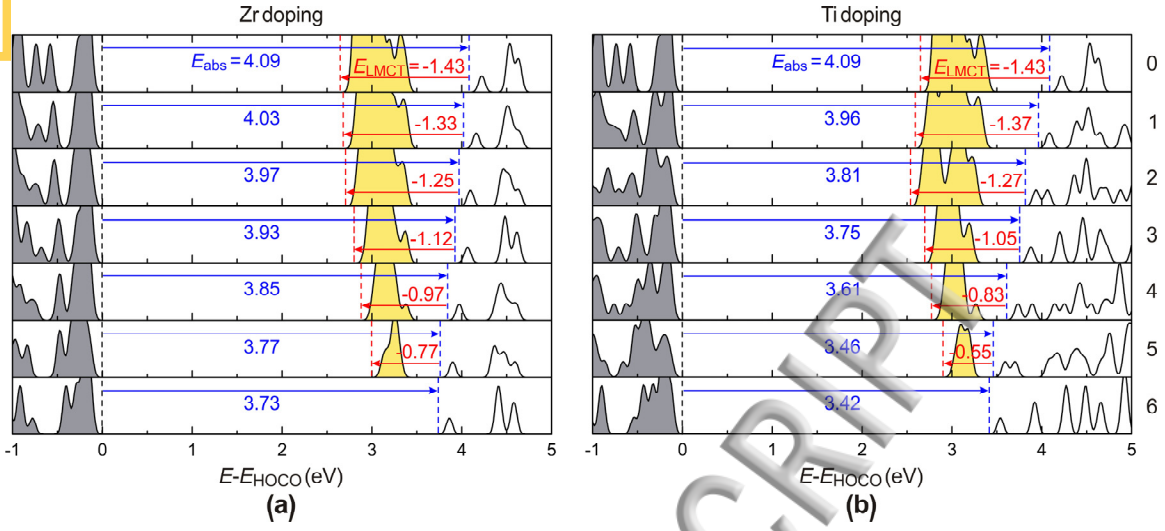

FIG. 4. Evolution of the density of states from Ce-UiO-66 to (a) Zr-UiO-66 and (b) Ti-UiO-66 upon metal doping. The numbers of doping ions (Zr or Ti ions) per node are given on the right. Only the spin-up manifold is shown. The occupied orbitals and the unoccupied 4*f* orbitals are filled with gray and yellow, respectively. The HOCO is on the linker in all cases. The LUCO is on Ce for the Ce-containing cases, on the linker for the Zr-UiO-66, and on both linker and Ti for Ti-UiO-66. The energy levels of the HOCO, the lowest unoccupied 4*f* orbital, and the lowest unoccupied linker orbital are indicated by black, red, and blue dashed lines, respectively. The blue and red arrows indicate E_{abs} and E_{LMCT}, respectively; the values of E_{abs} and E_{LMCT} are given as well.

The decrease of E_{abs} caused by doping might be accompanied by a decrease of the charge carrier lifetime because (i) E_{LMCT} is concomitantly raised and (ii) the number of Ce sites, which favor the charge separation, is decreased. Nevertheless, even at high doping concentrations, E_{LMCT} is still negative enough to favor charge separation. The mixed Ce/Ti-UiO-66 MOF is especially promising because ligand-to-Ti charge transfer can be promoted by Ti 3*d* orbitals overlapping effectively with the unoccupied linker orbitals (and the ligand-to-Ti charge-transfer energy is zero). The observed[44] long-lived photo-excited charges in Ti-MIL-125-NH_2 result from this kind of charge transfer.

D. Spectra and Electronic Properties with Functionalized Linkers

For water splitting, OER has much slower kinetics than HER.[58,59] For mixed-metal MOFs studied here, HER is expected to take place at the nodes if the excited electrons are transported from the linker to the metals via the LMCT process. Therefore, the overall efficiency of water splitting should not be very sensitive to the number of Ce ions when the Ce concentration is high enough for HER to proceed. We thus consider the $Ce_2Zr_4O_4(OH)_4$ and $Ce_2Ti_4O_4(OH)_4$ mixed-metal nodes having the (1,2,3,5) doping configuration because it offers two nearest neighbor Ce sites to perform HER (which is a two-electron transfer reaction).

Functionalizing the BDC linker can enhance the light harvesting capability of the MOF by lowering the E_{abs} of the linker.[43] In order to utilize the visible portion of the solar energy spectrum, we considered two types of functionalized linkers (see Figure 5), i.e., monosubstituted BDC (BDC-X) and disubstituted BDC (BDC-2,5-X), in mixed-metal MOFs; because they should be synthetically accessible,[60] we consider NH_2, NO_2, F, Cl, Br, I, OH, SH, COOH, CH_3, CF_3, and SO_3H as the substituents X.

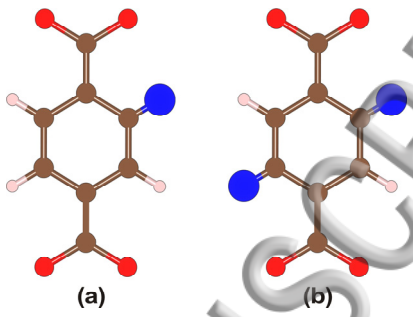

FIG. 5. The (a) BDC-X and (b) BDC-2,5-X linkers. The substituents X are in blue.

An initial screening of the light harvesting capabilities of the BDC-X and BDC-2,5-X linkers is conducted by simulating absorption spectra of their protonated structures, i.e., isolated H_2BDC-X and H_2BDC-2,5-X, based on the TD-DFT results of these protonated structures. The simulated absorption spectra are plotted in Figure 6, in which the spectrum of pristine H_2BDC species is also shown as a reference. The H_2BDC-2,5-X species show larger shifts toward the visible region than the corresponding H_2BDC-X species, consistent with a previous work.[43]

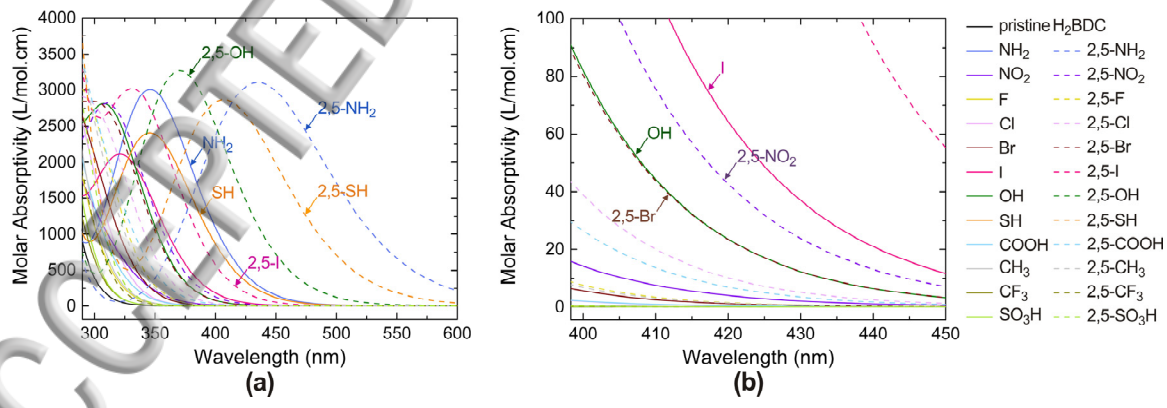

FIG. 6. Absorption spectra of the isolated H_2BDC, H_2BDC-X, and H_2BDC-2,5-X species. Note that (a) and (b) are same plots with different scales; (b) is an enlarged version of (a) showing only a portion of the visible region of the spectrum.

According to the spectra, the top ten visible-response species are H_2BDC-2,5-NH_2, H_2BDC-2,5-SH, H_2BDC-2,5-OH, H_2BDC-NH_2, H_2BDC-SH, H_2BDC-2,5-I, H_2BDC-I, H_2BDC-2,5-NO_2, H_2BDC-OH, and H_2BDC-2,5-Br. The corresponding linkers of these ten species are considered as potential candidates to combine with the $Ce_2Zr_4O_4(OH)_4$ and $Ce_2Ti_4O_4(OH)_4$ mixed-metal nodes as well as the $Ce_6O_4(OH)_4$ node. The density of states of the resulting 30 MOFs are reported in the Supplementary Material (i.e., Figures S4-S6).

Table III provides E_g, E_{abs}, and E_{LMCT} of these 30 MOFs. The table shows that linker functionalizations on Ce-UiO-66 lower the HOCO–LUCO gap and the E_{abs} of unfunctionalized Ce-UiO-66 because of new filled states within the original HOCO–LUCO gap of unfunctionalized Ce-UiO-66.[34,43] The lowering of E_{abs} is also consistent with the absorption spectra of the isolated linkers shown in Figure 6. In addition, the trend for visible-response abilities of isolated linkers predicted by the absorption spectra (Figure 6) correlates well with the E_{abs} results for the various functionalized Ce-UiO-66, and this confirms that the initial screening on isolated linkers is reliable. The E_{LMCT} of all functionalized Ce-UiO-66 are negative, but they show variations compared to the E_{LMCT} of unfunctionalized Ce-UiO-66, and this highlights the ability of substituents for tuning the E_{LMCT} and agrees with our previous work.[34] Moreover, Table III shows that, as expected, metal doping in functionalized Ce-UiO-66 MOFs opens the HOCO–LUCO gap, lowers the E_{abs}, and raises the E_{LMCT} of those MOFs.

TABLE III. HOCO–LUCO gaps (E_g, in eV), absorption energies (E_{abs}, in eV), and ligand-to-metal charge-transfer energies (E_{LMCT}, in eV) of Ce-UiO-66, Ce-UiO-66(Zr_4), and Ce-UiO-66(Ti_4) with various linker functionalizations

	Ce-UiO-66			Ce-UiO-66(Zr_4)			Ce-UiO-66(Ti_4)		
	E_g	E_{abs}	E_{LMCT}	E_g	E_{abs}	E_{LMCT}	E_g	E_{abs}	E_{LMCT}
2,5-NH_2	0.17	1.89	-1.72	0.39	1.58	-1.19	0.31	1.27	-0.97
2,5-SH	0.09	1.82	-1.73	0.62	1.78	-1.16	0.43	1.34	-0.91
2,5-OH	0.33	2.11	-1.78	0.56	1.86	-1.30	0.41	1.40	-0.99
NH_2	1.17	2.74	-1.57	1.37	2.48	-1.11	1.22	2.14	-0.92
SH	0.95	2.54	-1.59	1.27	2.37	-1.09	1.12	2.04	-0.92
2,5-I	1.26	2.76	-1.50	1.48	2.48	-0.99	1.30	2.13	-0.83
I	1.53	2.97	-1.44	1.76	2.76	-0.99	1.65	2.55	-0.90
2,5-NO_2	2.13	3.19	-1.06	2.35	3.02	-0.67	2.30	2.93	-0.63
OH	1.41	3.02	-1.61	1.64	2.77	-1.13	1.51	2.44	-0.92
2,5-Br	1.72	3.16	-1.44	1.97	2.95	-0.98	1.83	2.66	-0.83

E. Screening of Visible-Response Water Splitting Photocatalysts

The standard electrode potentials of the HER and the OER are 0 and 1.23 V, respectively,[61] therefore the lower limit for E_g is 1.23 eV (energy difference of the HER and the OER levels) plus an 0.25 eV[62] or more[2] for the overpotential required to drive the HER and the OER, that is,

E_g has a lower limit of 1.48 eV. Because we are interested in visible-response photocatalysts, we eliminated the MOFs with E_{abs} larger than 3.0 eV. Nine MOFs remain for consideration, and they are identified in Figure 7.

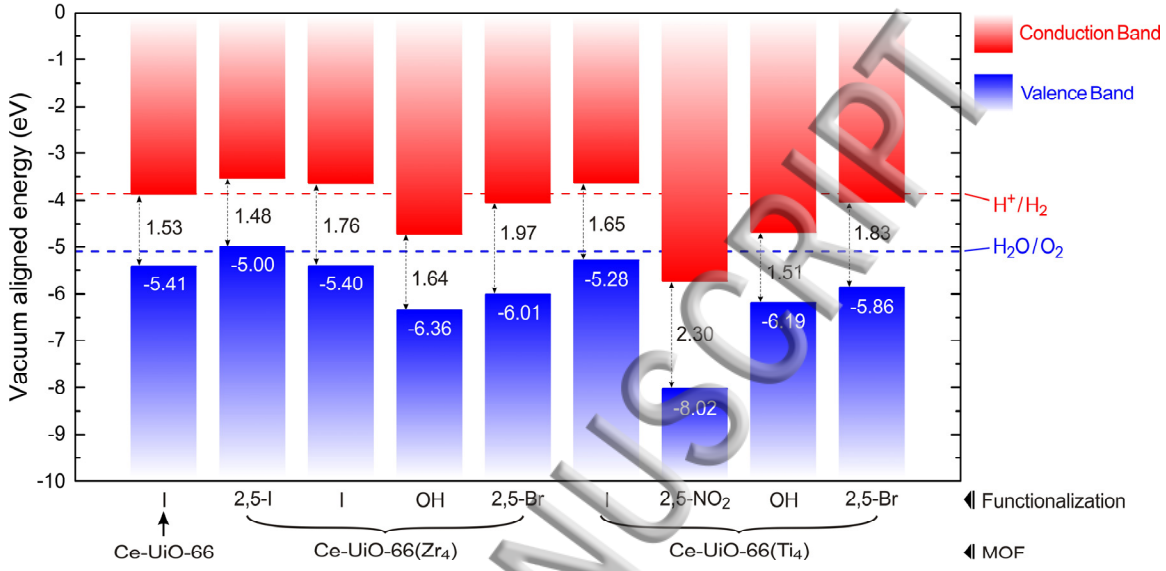

FIG. 7. Band alignment of Ce-UiO-66, Ce-UiO-66(Zr_4), and Ce-UiO-66(Ti_4) with linker functionalizations. For each case, the HOCO and the LUCO are from the linker and the Ce, respectively. The red and blue dashed lines represent energy levels corresponding to redox potentials for water splitting (pH = 7; T = 298.15 K). The band gaps (black numbers) and the vacuum aligned HOCO energies (white numbers) are given as well.

The absolute band edges (i.e., HOCO and LUCO positions with respect to the vacuum level) of a photocatalyst are necessary to predict the thermodynamic feasibility of the photocatalytic water splitting reaction. At pH = 7 and room temperature (298.15 K), the HER level is located at -3.87 eV and the OER level is located at -5.09 eV, with respect to the vacuum level.[34] Figure 7 shows the vacuum aligned energies of the HOCO and the LUCO of the nine candidates corresponding to the positions of the HER and the OER levels at pH = 7 and room temperature. The three MOFs with the BDC-I linker basically have appropriate LUCO and HOCO positions to straddle the HER and the OER levels. Of these, Ce-UiO-66(Ti_4)-I is the most promising visible-response photocatalyst for water splitting using a single photocatalyst because Table III shows that it has E_{abs} equal to 2.55 eV. Among the nine candidates, Ce-UiO-66(Zr_4)-2,5-I and Ce-UiO-66(Ti_4)-OH also have E_{abs} equal approximately to 2.5 eV (see Table III). However, the LUCO position of Ce-UiO-66(Ti_4)-OH is too low in energy to drive the HER. The HOCO position of Ce-UiO-66(Zr_4)-2,5-I is slightly above the OER level, and this small deviation can be corrected by applying a weak external bias voltage to shift both the HOCO and the LUCO positions (note that the external bias voltage should not be too large as it also consumes energy), so Ce-UiO-66(Zr_4)-2,5-I is also a potential visible-response photocatalyst for water splitting using a single

photocatalyst. It is also interesting to note that the pure Ce version of Ce-UiO-66(Zr_4)-2,5-I, i.e., Ce-UiO-66-2,5-I, has a too small HOCO–LUCO gap (1.26 eV) for water splitting, while with Zr doping, the HOCO–LUCO gap is increased to 1.48 eV, which is adequate to drive the water splitting reaction.

IV. CONCLUSIONS

We studied metal doping in Ce-UiO-66 using Zr or Ti as dopant. Possible doping configurations were investigated, and the most stable doping configurations for different doping concentrations were determined. The solid stability of the mixed-metal MOFs (mixed Ce/Zr-UiO-66 and mixed Ce/Ti-UiO-66) and the synthetic feasibility of the hypothetical mixed Ce/Ti-UiO-66 MOFs were then discussed. We expect that the hypothetical mixed Ce/Ti-UiO-66 MOFs are synthetically accessible because their energies of mixing are small and because CeO_2-TiO_2 solid solutions can be synthesized.

Inspection of the electronic structures of the mixed-metal MOFs (having the most stable doping configurations) shows that doping Ce-UiO-66 with Zr or Ti can raise the too negative E_{LMCT} (-1.43 eV) of Ce-UiO-66, which is necessary for water splitting using a single photocatalyst that is based on Ce-MOFs and that absorbs in the visible region,[34] because the raised E_{LMCT} contributes to the decrease of E_{abs}, enhancing the light harvesting capability. We found that Zr or Ti doping in Ce-UiO-66 can tune the HOCO–LUCO gap as well; for Zr doping, the gap is opened at any Zr doping concentration; for Ti doping, the gap is slightly lowered at low doping concentration, while it is opened when the Ti:Ce ratio is equal to or greater than 1.

We also explored linker functionalization of the Ce-UiO-66 pure-metal MOF and the Ce-UiO-66(Zr_4) and Ce-UiO-66(Ti_4) mixed-metal MOFs. We found that Ce-UiO-66(Ti_4)-I is the most promising visible-response photocatalyst considered for water splitting using a single photocatalyst and that Ce-UiO-66(Zr_4)-2,5-I is also a promising material, although it may require a weak external bias voltage to slightly shift its HOCO and LUCO positions.

SUPPLEMENTARY MATERIAL

See supplementary material for the electronic structures of Ce-UiO-66(M_3) where M = Zr or Ti; M-UiO-66 where M = Zr or Ti or Ce; functionalized Ce-UiO-66; functionalized Ce-UiO-66(Zr_4); functionalized Ce-UiO-66(Ti_4), the calculated absolute energies, and the coordinates of the systems studied.

ACKNOWLEDGMENTS

This research was supported as part of the Nanoporous Materials Genome Center by the U.S. Department of Energy, Office of Basic Energy Sciences, Division of Chemical Sciences, Geosciences, and Biosciences under award DE-FG02-17ER16362.

[1] W. Lubitz and W. Tumas, Chem. Rev. **107**, 3900 (2007).

[2] M. G. Walter, E. L. Warren, J. R. McKone, S. W. Boettcher, Q. Mi, E. A. Santori, and N. S. Lewis, Chem. Rev. **110**, 6446 (2010).

[3] K. Maeda and K. Domen, J. Phys. Chem. Lett. **1**, 2655 (2010).

[4] C. Acar, I. Dincer, and G. F. Naterer, Int. J. Energy Res. **40**, 1449 (2016).

[5] T. Jafari, E. Moharreri, A. S. Amin, R. Miao, W. Song, and S. L. Suib, Molecules **21**, 900 (2016).

[6] A. Kudo and Y. Miseki, Chem. Soc. Rev. **38**, 253 (2009).

[7] J. Schneider, M. Matsuoka, M. Takeuchi, J. Zhang, Y. Horiuchi, M. Anpo, and D. W. Bahnemann, Chem. Rev. **114**, 9919 (2014).

[8] F. Fresno, R. Portela, S. Suárez, and J. M. Coronado, J. Mater. Chem. A **2**, 2863 (2014).

[9] K. Meyer, M. Ranocchiari, and J. A. van Bokhoven, Energy Environ. Sci. **8**, 1923 (2015).

[10] H. Wang, Q.-L. Zhu, R. Zou, and Q. Xu, Chem **2**, 52 (2017).

[11] O. M. Yaghi, H. Li, C. Davis, D. Richardson, and T. L. Groy, Acc. Chem. Res. **31**, 474 (1998).

[12] V. Bernales, M. A. Ortuño, D. G. Truhlar, C. J. Cramer, and L. Gagliardi, ACS Cent. Sci. **4**, 5 (2018).

[13] D. Britt, D. Tranchemontagne, and O. M. Yaghi, Proc. Natl. Acad. Sci. U. S. A. **105**, 11623 (2008).

[14] K. Sumida, D. L. Rogow, J. A. Mason, T. M. McDonald, E. D. Bloch, Z. R. Herm, T.-H. Bae, and J. R. Long, Chem. Rev. **112**, 724 (2012).

[15] N. C. Burtch, H. Jasuja, and K. S. Walton, Chem. Rev. **114**, 10575 (2014).

[16] J. H. Cavka, S. Jakobsen, U. Olsbye, N. Guillou, C. Lamberti, S. Bordiga, and K. P. Lillerud, J. Am. Chem. Soc. **130**, 13850 (2008).

[17] C. Wang, X. Liu, N. K. Demir, J. P. Chen, and K. Li, Chem. Soc. Rev. **45**, 5107 (2016).

[18] S. Jakobsen, D. Gianolio, D. S. Wragg, M. H. Nilsen, H. Emerich, S. Bordiga, C. Lamberti, U. Olsbye, M. Tilset, and K. P. Lillerud, Phys. Rev. B **86**, 125429 (2012).

[19] C. Falaise, C. Volkringer, J.-F. Vigier, N. Henry, A. Beaurain, and T. Loiseau, Chem. Eur. J. **19**, 5324 (2013).

[20] M. Lammert, M. T. Wharmby, S. Smolders, B. Bueken, A. Lieb, K. A. Lomachenko, D. D. Vos, and N. Stock, Chem. Commun. **51**, 12578 (2015).

[21] C. Falaise, A. Assen, I. Mihalcea, C. Volkringer, A. Mesbah, N. Dacheux, and T. Loiseau, Dalton Trans. **44**, 2639 (2015).

[22] C. Falaise, J.-S. Charles, C. Volkringer, and T. Loiseau, Inorg. Chem. **54**, 2235 (2015).

[23] D. Sun, W. Liu, M. Qiu, Y. Zhang, and Z. Li, Chem. Commun. **51**, 2056 (2015).

[24] Y. Lee, S. Kim, J. K. Kang, and S. M. Cohen, Chem. Commun. **51**, 5735 (2015).

[25] F. Nouar, M. I. Breeze, B. C. Campo, A. Vimont, G. Clet, M. Daturi, T. Devic, R. I. Walton, and C. Serre, Chem. Commun. **51**, 14458 (2015).

[26] A. S. Yasin, J. Li, N. Wu, and T. Musho, Phys. Chem. Chem. Phys. **18**, 12748 (2016).

[27] A. Wang, Y. Zhou, Z. Wang, M. Chen, L. Sun, and X. Liu, RSC Adv. **6**, 3671 (2016).

[28] J. Tu, X. Zeng, F. Xu, X. Wu, Y. Tian, X. Hou, and Z. Long, Chem. Commun. **53**, 3361 (2017).

[29] M. Lammert, C. Glißmann, and N. Stock, Dalton Trans. **46**, 2425 (2017).

[30] A. S. Portillo, H. G. Baldoví, M. T. G. Fernandez, S. Navalón, P. Atienzar, B. Ferrer, M. Alvaro, H. Garcia, and Z. Li, J. Phys. Chem. C **121**, 7015 (2017).

[31] C. G. Silva, I. Luz, F. X. Llabrés i Xamena, A. Corma, and H. García, Chem. Eur. J. **16**, 11133 (2010).

[32] Y.-P. Yuan, L.-S. Yin, S.-W. Cao, G.-S. Xu, C.-H. Li, and C. Xue, Appl. Catal. B **168-169**, 572 (2015).

[33] J.-D. Xiao, Q. Shang, Y. Xiong, Q. Zhang, Y. Luo, S.-H. Yu, and H.-L. Jiang, Angew. Chem. Int. Ed. **55**, 9389 (2016).

[34] X.-P. Wu, L. Gagliardi, and D. G. Truhlar, J. Am. Chem. Soc. (2018); online at DOI: 10.1021/jacs.8b03613

[35] K. Hendrickx, J. J. Joos, A. De Vos, D. Poelman, P. F. Smet, V. Van Speybroeck, P. Van Der Voort, and K. Lejaeghere, Inorg. Chem. **57**, 5463 (2018).

[36] G. Dutta, U. V. Waghmare, T. Baidya, M. S. Hegde, K. R. Priolkar, and P. R. Sarode, Chem. Mater. **18**, 3249 (2006).

[37] T. Montini, M. Melchionna, M. Monai, and P. Fornasiero, Chem. Rev. **116**, 5987 (2016).

[38] G. Kresse and J. Hafner, Phys. Rev. B **49**, 14251 (1994).

[39] G. Kresse and J. Furthmüller, Comput. Mater. Sci. **6**, 15 (1996).

[40] J. P. Perdew, A. Ruzsinszky, G. I. Csonka, O. A. Vydrov, G. E. Scuseria, L. A. Constantin, X. Zhou, and K. Burke, Phys. Rev. Lett. **100**, 136406 (2008).

[41] A. V. Krukau, O. A. Vydrov, A. F. Izmaylov, and G. E. Scuseria, J. Chem. Phys. **125**, 224106 (2006).

[42] P. E. Blöchl, Phys. Rev. B **50**, 17953 (1994).

[43] K. Hendrickx, D. E. P. Vanpoucke, K. Leus, K. Lejaeghere, A. Van Yperen-De Deyne, V. Van Speybroeck, P. Van Der Voort, and K. Hemelsoet, Inorg. Chem. **54**, 10701 (2015).

[44] M. A. Nasalevich, C. H. Hendon, J. G. Santaclara, K. Svane, B. van der Linden, S. L. Veber, M. V. Fedin, A. J. Houtepen, M. A. van der Veen, F. Kapteijn, A. Walsh, and J. Gascon, Sci. Rep. **6**, 23676 (2016).

[45] K. T. Butler, C. H. Hendon, and A. Walsh, J. Am. Chem. Soc. **136**, 2703 (2014).

[46] M. J. Frisch, G. W. Trucks, H. B. Schlegel, G. E. Scuseria, M. A. Robb, J. R. Cheeseman, G. Scalmani, V. Barone, G. A. Petersson, H. Nakatsuji, X. Li, M. Caricato, A. V. Marenich, J. Bloino, B. G. Janesko, R. Gomperts, B. Mennucci, H. P. Hratchian, J. V. Ortiz, A. F. Izmaylov, J. L. Sonnenberg, D. Williams-Young, F. Ding, F. Lipparini, F. Egidi, J. Goings, B. Peng, A. Petrone, T. Henderson, D. Ranasinghe, V. G. Zakrzewski, J. Gao, N. Rega, G. Zheng, W. Liang, M. Hada, M. Ehara, K. Toyota, R. Fukuda, J. Hasegawa, M. Ishida, T. Nakajima, Y. Honda, O. Kitao, H. Nakai, T. Vreven, K. Throssell, J. A. Montgomery, Jr., J. E. Peralta, F. Ogliaro, M. J. Bearpark, J. J. Heyd, E. N. Brothers, K. N. Kudin, V. N. Staroverov, T. A. Keith, R. Kobayashi, J. Normand, K. Raghavachari, A. P. Rendell, J. C. Burant, S. S. Iyengar, J. Tomasi, M. Cossi, J. M. Millam, M. Klene, C. Adamo, R. Cammi, J. W. Ochterski, R. L. Martin, K. Morokuma, O. Farkas, J. B. Foresman, and D. J. Fox, *Gaussian 16*, *Revision A.03*, Gaussian, Inc., Wallingford CT, 2016.

[47] M. E. Casida, C. Jamorski, K. C. Casida, D. R. Salahub, J. Chem. Phys. **108**, 4439 (1998).

[48] F. Weigend and R. Ahlrichs, Phys. Chem. Chem. Phys. **7**, 3297 (2005).

[49] F. Weigend, Phys. Chem. Chem. Phys. **8**, 1057 (2006).

[50] R. Dennington, T. A. Keith, and J. M. Millam, *GaussView*, *Version 6*, Semichem, Inc., Shawnee Mission, KS, 2016. See http://gaussian.com/uvvisplot.

[51] A. Kuc, A. Enyashin, and G. Seifert, J. Phys. Chem. B **111**, 8179 (2007).

[52] L.-M. Yang, P. Vajeeston, P. Ravindran, H. Fjellvåg, and M. Tilset, Phys. Chem. Chem. Phys. **13**, 10191 (2011).

[53] L.-M. Yang, E. Ganz, S. Svelle, and M. Tilset, J. Mater. Chem. C **2**, 7111 (2014).

[54] J. Z. Liu and A. Zunger, Phys. Rev. B **77**, 205201 (2008).

[55] E. Zhao, J. Meng, Y. Ma, and Z. Wu, Phys. Chem. Chem. Phys. **12**, 13158 (2010).

[56] F. Trousselet, A. Archereau, A. Boutin, and F.-X. Coudert, J. Phys. Chem. C **120**, 24885 (2016).

[57] D. A. Porter and K. E. Easterling, *Phase Transformations in Metals and Alloys*, 2nd ed. (Springer, New York, 1992), p. 15.

[58] A. J. Nozik, Nature **257**, 383 (1975).

[59] M. P. Dare-Edwards, J. B. Goodenough, A. Hamnett, and P. R. Trevellick, J. Chem. Soc. Faraday Trans. 1 **79**, 2027 (1983).

[60] Z. Hu and D. Zhao, Dalton Trans. **44**, 19018 (2015).

[61] *CRC Handbook of Chemistry and Physics*, 92nd ed.; W. M. Haynes, Ed.; CRC Press: Boca Raton, FL, 2011; pp. 5-82–5-83.

[62] M. S. Wrighton, D. S. Ginley, P. T. Wolczanski, A. B. Ellis, D. L. Morse, and A. Linz, Proc. Natl. Acad. Sci. U. S. A. **72**, 1518 (1975).

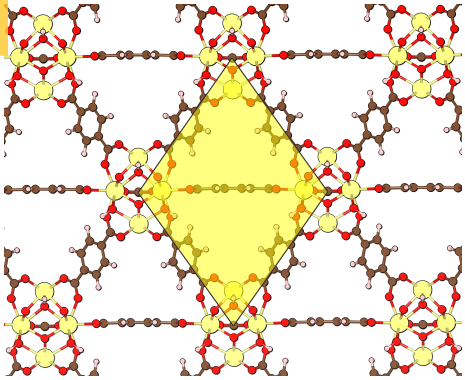

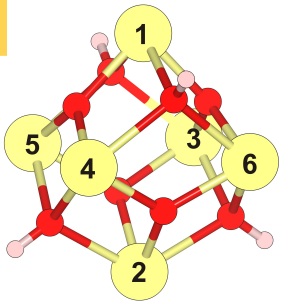

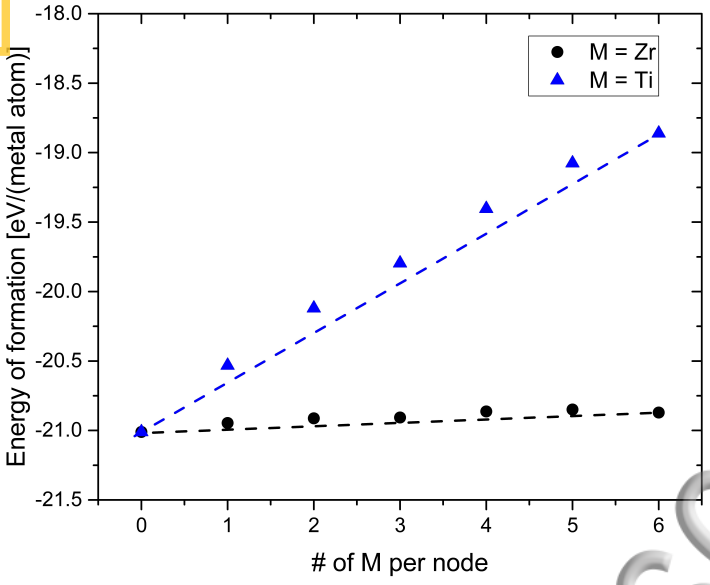

This manuscript was accepted by J. Chem. Phys. Click here to see the version of record.

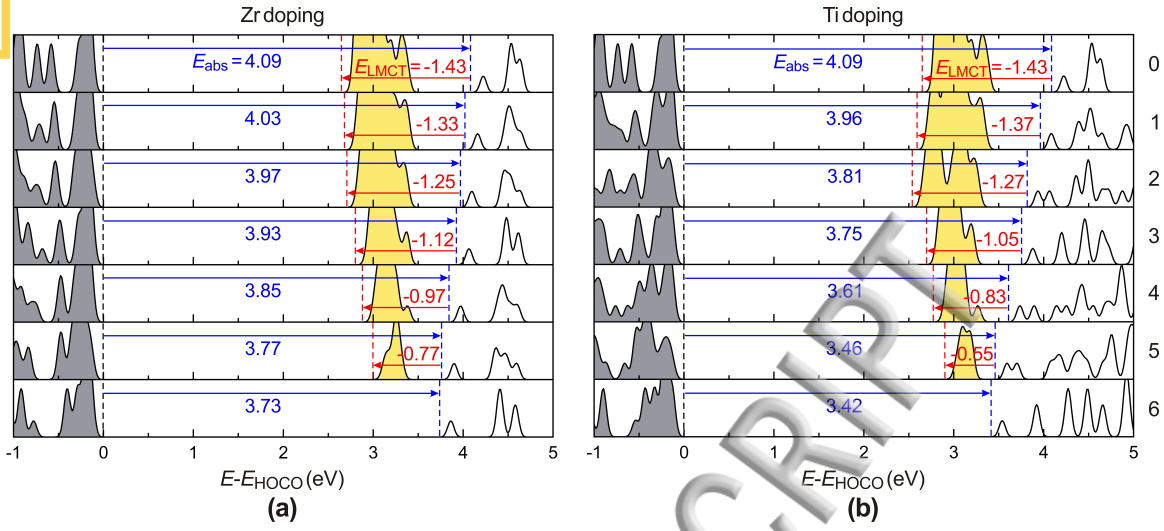

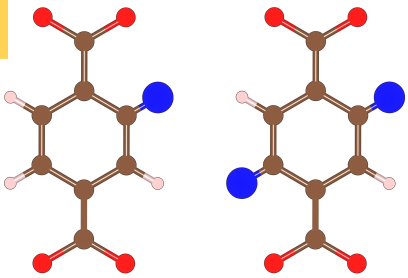

(a) (b)

This manuscript was accepted by J. Chem. Phys. Click here to see the version of record.